

# Nonlinear excitation of low- $n$ harmonics in reduced magnetohydrodynamic simulations of edge-localized modes

I. Krebs<sup>1</sup>, M. Hölzl<sup>1</sup>, K. Lackner<sup>1</sup>, S. Günter<sup>1</sup>

<sup>1</sup>Max Planck Institute for Plasma Physics, EURATOM Association, Boltzmannstr. 2, 85748 Garching, Germany

## Abstract

Nonlinear simulations of the early ELM phase based on a typical type-I ELMy ASDEX Upgrade discharge have been carried out using the reduced MHD code JOEKE. The analysis is focused on the evolution of the toroidal Fourier spectrum. It is found that during the nonlinear evolution, linearly subdominant low- $n$  Fourier components, in particular the  $n = 1$ , grow to energies comparable with linearly dominant harmonics. A simple model is developed, based on the idea that energy is transferred among the toroidal harmonics via second order nonlinear interaction. The simple model reproduces and explains very well the early nonlinear evolution of the toroidal spectrum in the JOEKE simulations. Furthermore, it is shown for the  $n = 1$  harmonic, that its spatial structure changes significantly during the transition from linear to nonlinearly driven growth. The rigidly growing structure of the linearly barely unstable  $n = 1$  reaches far into the plasma core. In contrast, the nonlinearly driven  $n = 1$  has a rigidly growing structure localized at the plasma edge, where the dominant toroidal harmonics driving the  $n = 1$  are maximal and in phase. The presented quadratic coupling model might explain the recent experimental observation of strong low- $n$  components in magnetic measurements [Wenninger et al., *Non-linear magnetic perturbations during edge localized modes in TCV dominated by low  $n$  mode components*, submitted to Nuclear Fusion].

## 24 **1 Introduction**

25 Edge-localized modes (ELMs) are relaxation-oscillation instabilities observed at the edge of  
26 tokamak plasmas in high-confinement regime (H-mode). Ejecting energy and particles from the  
27 plasma, ELMs have the favorable effect of reducing the impurity content of the plasma and pro-  
28 viding a mean to control the plasma density [1]. But if too large, they cause large heat fluxes  
29 which can damage plasma facing components [2, 3]. As the ability of controlling the ELM prop-  
30 erties decides on whether the H-mode can be a suitable operational regime for ITER and future  
31 fusion reactors, the understanding of this instability is crucial. Nonlinear MHD simulations are  
32 an important tool in the quest for theoretical comprehension of ELMs.

33 A nonlinear reduced MHD code which has been developed especially for edge instabilities, is  
34 the JOREK code [4]. In this work, it is used for simulations of the early ELM phase, which are  
35 based on the geometry and parameters of an ASDEX Upgrade tokamak [?] discharge. Section  
36 2 introduces JOREK and gives details about the simulations. The toroidal Fourier spectrum of  
37 the instability and its nonlinear evolution is analyzed and compared to recent experimental find-  
38 ings in Section 3. It is observed, that initially weakly unstable toroidal Fourier components can  
39 become important nonlinearly. In Section 4, the question is addressed, what determines the non-  
40 linear evolution of the toroidal harmonics in the simulations. A simple model is presented that  
41 shows how this evolution can be understood in the framework of second order nonlinear cou-  
42 pling between the toroidal harmonics. Finally, in Section 5 it is investigated how the radial and  
43 poloidal localization of a linearly subdominant toroidal harmonic changes due to its nonlinearly  
44 driven growth. A summary and an outlook are given in Section 6.

## 45 **2 The JOREK code and the simulations**

### 46 **JOREK**

47 The finite element code JOREK solves the nonlinear reduced MHD equations in full toroidal  
48 X-point geometry including separatrix and open flux surfaces. JOREK has originally been de-  
49 veloped by G.T.A. Huysmans [6, 7]. For the presented simulations, a single fluid version of  
50 JOREK<sup>1</sup> ("model302") has been used. The code is discretized via a Fourier decomposition in  
51 toroidal direction and 2D bi-cubic Bézier finite elements in the poloidal plane. The grid in the  
52 poloidal plane is aligned to the flux surfaces and can be refined in the regions of interest. The  
53 toroidal Fourier decomposition allows to choose the toroidal harmonics included in the compu-  
54 tation. The discretization in time is performed according to a fully implicit Crank-Nicholson

---

<sup>1</sup>The used code revision is R706.

55 scheme. For the part of the boundary which follows the outermost open flux surface, ideally  
 56 conducting wall boundary conditions are implemented, and for the divertor where the bound-  
 57 ary is crossed by magnetic field lines, modified Bohm boundary conditions apply. The code  
 58 uses a particular normalization of the physical variables. A JOREK time unit corresponds to  
 59 approximately  $0.5 \mu\text{s}$  at the parameters of the presented simulations. In the following, quantities  
 60 indexed with "JOREK" are normalized according to the JOREK normalization scheme (units of  
 61 these quantities are omitted). For the equations solved by the applied JOREK model and details  
 62 about the normalization of the variables, please refer to Reference [8].

## 63 The simulations

64 The simulations are focused on the early ELM phase when the instability grows exponentially  
 65 before the onset of nonlinear saturation. Emphasis has been put on the analysis of the nonlinear  
 66 interaction of the toroidal Fourier harmonics, thus a large number of included toroidal harmon-  
 67 ics and a high flexibility in combining them was required. The simulations are based on the  
 68 simulations presented in Reference [8]<sup>2</sup> with an additional modification of the code providing  
 69 the possibility of excluding desired harmonics from the simulation. The baseline simulation  
 70 includes 16 toroidal Fourier harmonics  $n = 1, 2, \dots, 16$  in addition to the axisymmetric  $n = 0$   
 71 part. To analyze the interaction of the different harmonics in more detail, a large number of  
 72 simulations including different subsets of these harmonics has been carried out.

73 The simulations are based on an equilibrium reconstruction of a typical type-I ELMy H-mode  
 74 ASDEX Upgrade discharge (#23221 at 4.7 s). The equilibrium reconstruction has been per-  
 75 formed with the CLISTE code [9, 10]. The corresponding equilibrium pressure and safety factor  
 76 profiles are shown in Figure 1. The particle density in the plasma center is  $6 \cdot 10^{19} \text{m}^{-3}$ . Heat  
 77 and particle sources and perpendicular heat and particle diffusivities are chosen such that the  
 78 background profiles do not change significantly during the simulation. The parallel particle dif-  
 79 fusivity is set to zero, parallel particle transport is thus provided by convection only. The heat  
 80 diffusion anisotropy at the separatrix is about  $\kappa_{\parallel}/\kappa_{\perp} = 7 \cdot 10^6$ . Viscosity and resistivity have a  
 81  $T_N^{-3/2}$  temperature dependency where  $T_N$  is the temperature normalized by its value at the plasma  
 82 center. The core viscosity is set to about  $1.2 \cdot 10^{-5} \text{kgm}^{-1} \text{s}^{-1}$ . The resistivity ( $\eta \approx 5 \cdot 10^{-5} \Omega\text{m}$   
 83 in the core, leading to a Lundquist number of about  $10^5$ ) is larger than in a realistic ASDEX  
 84 Upgrade discharge<sup>3</sup> due to computational restrictions.

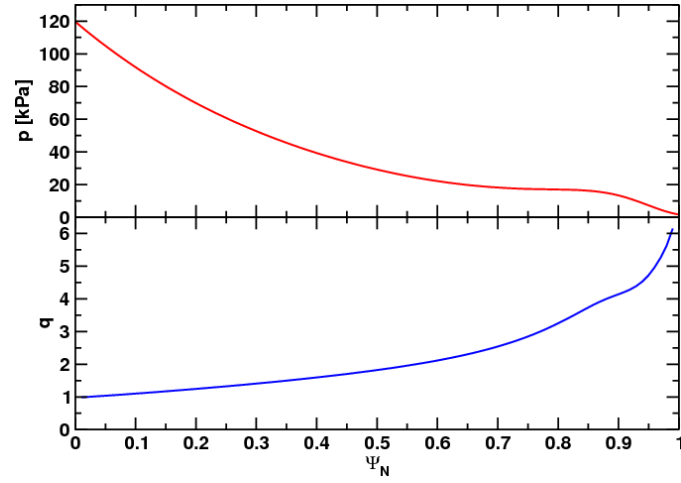


Figure 1: Equilibrium pressure (red) and safety factor (blue), obtained from an equilibrium reconstruction of an ASDEX Upgrade discharge. The values of the safety factor in the center and at the edge are  $q(0) \approx 1$  and  $q(0.95) \approx 4.7$ .

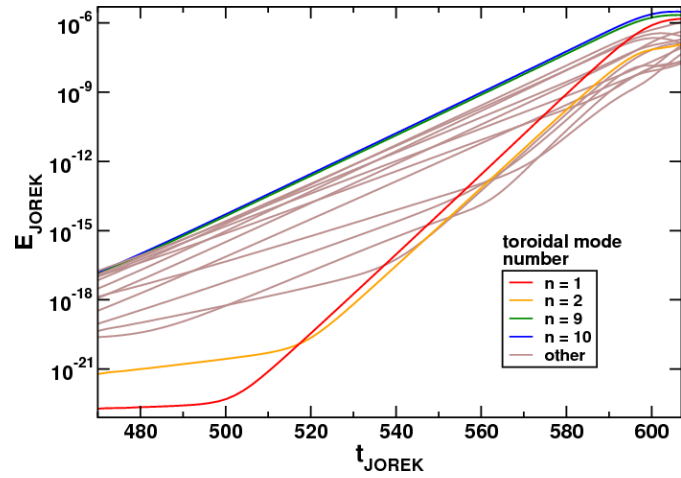


Figure 2: Time evolution of the energies contained in the different toroidal Fourier harmonics in the early ELM phase of a simulation with included mode numbers  $n = 1, 2, \dots, 16$ . The linearly dominant harmonics are  $n = 9$  and  $n = 10$ . Energy is transferred from the dominant to the linearly subdominant harmonics, like  $n = 1$  or  $n = 2$ , by nonlinear interaction.

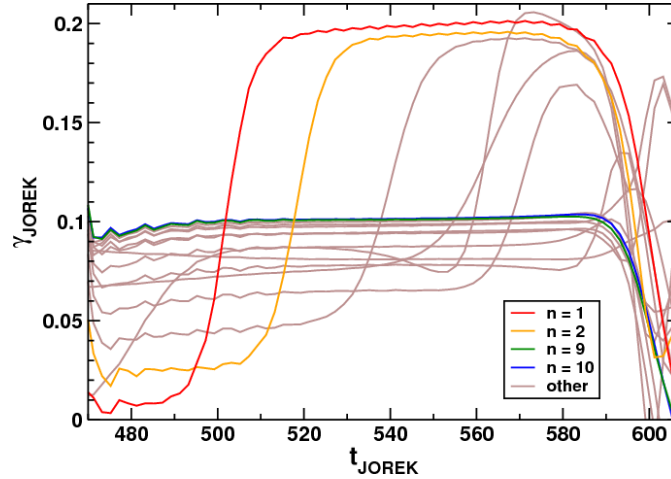


Figure 3: Growth rates of the toroidal Fourier harmonics in a simulation with  $n = 1, 2, \dots, 16$ . In the linear phase at the beginning of the exponential growth of the perturbation, the harmonics grow at constant growth rates and independently of each other. Subsequently, the growth rates of the linearly subdominant harmonics increase due to nonlinear interaction between the different toroidal harmonics. At the end of this early nonlinear phase, the growth begins to saturate.

### 3 Nonlinear evolution of the toroidal harmonics

The time evolution of the toroidal Fourier harmonics of the perturbation in the early phase of an ELM can be subdivided into three phases, a linear phase, an early nonlinear phase and the nonlinear saturation. Time traces of total energies and growth rates of the different toroidal harmonics in a simulation with 16 included harmonics ( $n = 1, 2, \dots, 16$ ) are shown in Figures 2 and 3.

At the beginning of the exponential growth of the instability, the toroidal harmonics grow at a constant rate. The growth rate of a toroidal Fourier component in this linear phase of the evolution is the same as in a simulation where this component is the only included one. It is observed that in the linear phase of this simulation, the Fourier components with mode numbers  $n = 9$  and  $n = 10$  grow the fastest. In our simulations, diamagnetic drift effects are neglected which would act stabilizing on high- $n$  harmonics. However, the poloidal resolution limited by computational restrictions also reduces the growth rates of harmonics with high mode numbers. Linearly dominant mode numbers in the intermediate range, as we observe them here, are thus in line with linear theory again.

<sup>2</sup>The same equilibrium and parameters as in the "eta5" simulation in Reference [8] have been used here.

<sup>3</sup>The core resistivity in ASDEX Upgrade discharges has values of about  $10^{-8} \Omega\text{m}$ .

100 In contrast to the linear phase where the toroidal Fourier harmonics grow independently of each  
 101 other, the harmonics start to interact in the subsequent early nonlinear phase. Due to nonlinear  
 102 interactions, energy is transferred among the toroidal Fourier components which influences their  
 103 growth rates. Following this phase, the nonlinear saturation yields a decrease of the growth rates.  
 104 The main saturation effect is, that the background current density and pressure gradient at the  
 105 edge are reduced by the perturbation, which weakens the drive of the instability. Additionally,  
 106 the stabilizing influence of the ideal wall boundary conditions becomes more important if the  
 107 displacement of the plasma due to the perturbation becomes significant compared to the distance  
 108 between separatrix and ideal wall.

109 In the following, emphasis is put on the dynamics of the early nonlinear phase before the onset  
 110 of saturation. It is observed that during this phase, growth rates of toroidal Fourier components  
 111 which are linearly subdominant increase and that in particular the  $n = 1$  toroidal harmonic even  
 112 reaches energies comparable to those of the linearly dominant components, which has already  
 113 been pointed out in [8]. This relates to very recent experimental observations. During type-I  
 114 ELMy discharges in TCV (Tokamak à configuration variable) the toroidal mode structure of the  
 115 magnetic perturbations has been found to be often dominated by low mode numbers, in particular  
 116 by the  $n = 1$  component [11]. The magnetic diagnostics in ASDEX Upgrade are not suitable for  
 117 the detection of low- $n$  harmonics<sup>4</sup> such that it is unclear at present if this phenomenon is also  
 118 found here.

## 119 4 Simple quadratic coupling model

120 The detailed dynamics of the early nonlinear phase, i.e., why the growth rates of the initially  
 121 subdominant toroidal harmonics increase, at which point in time the rise occurs and how large  
 122 the growth rates become, can be explained in the framework of "three wave interaction". Con-  
 123 sidering a superposition of two toroidal harmonics with mode numbers  $i$  and  $j$ , a second order  
 124 nonlinear term generates harmonics with mode numbers  $|i \pm j|$ . Hence, energy can be trans-  
 125 ferred to other harmonics by quadratic coupling. Based on this idea, a simple model describing  
 126 the time evolution of the amplitudes<sup>5</sup>  $A_i$  of the  $i^{\text{th}}$  toroidal harmonics can be set up by

$$\frac{\partial A_i}{\partial t} = \gamma_i A_i + \sum_{j=1}^{16} \sum_{k=1}^{16} \gamma_{jk}^i A_j A_k \delta(i \pm j \pm k) \quad \text{for } i = 1, 2, \dots, 16 \quad (1)$$

<sup>4</sup>The pick-up coils in ASDEX Upgrade cover only a part of the toroidal circumference. Full coverage would be required to resolve an  $n=1$  component, as the growth rate of the mode is comparable to the rotation frequency. Moreover, the pick-up coils measure the time derivative of the magnetic field perturbation which reduces the contribution of low- $n$  harmonics to the signal.

<sup>5</sup> $A_i$  is defined as  $\sqrt{E_i}$ , where  $E_i$  is the total energy contained in the  $i^{\text{th}}$  toroidal harmonic.

127 where  $\gamma_i$  are the constant linear growth rates and  $\gamma_{jk}^i$  are the coupling constants. As the latter  
 128 describe the spatial overlap of harmonics  $j$  and  $k$  in the poloidal plane, they can be set constant  
 129 assuming that the toroidal harmonics grow rigidly without changing their spatial structure. This  
 130 is indeed the case for all linearly dominant harmonics. The set of coupled nonlinear differential  
 131 equations (1) is able to reproduce to a large extent the time evolution of the toroidal Fourier  
 132 spectrum of the perturbation in the early nonlinear phase of the JOREK simulations. To achieve  
 133 this, the appropriate linear growth rates and coupling constants have to be chosen.

134 The linear growth rates  $\gamma_i$  can be extracted directly from the linear phase of the JOREK simula-  
 135 tions. From simulations with only few included toroidal harmonics, e.g., two linearly dominant  
 136 ones which nonlinearly drive a third harmonic, the relevant coupling constants can be isolated.  
 137 Six coupling constants remain, namely  $\gamma_{9,10}^1$ ,  $\gamma_{8,10}^2$ ,  $\gamma_{7,10}^3$ ,  $\gamma_{6,10}^4$ ,  $\gamma_{7,8}^{15}$  and  $\gamma_{7,9}^{16}$ .

138 Whereas the linear terms of Equations (1) cause an influx of energy into the system (from the  
 139 axisymmetric  $n = 0$  part), the nonlinear terms only yield an exchange of energy among the  
 140 toroidal harmonics and should thus conserve the total energy. If this conservation of energy is  
 141 taken into account, for each non-zero  $\gamma_{jk}^i$  also  $\gamma_{ik}^j$  and  $\gamma_{ij}^k$  have to be included into the model and

$$\frac{\partial E_{\text{tot}}}{\partial t} = \frac{\partial}{\partial t} \sum_i A_i^2 \stackrel{!}{=} 0 \quad (2)$$

142 has to be fulfilled at any time by the system of equations (1) omitting the linear terms. Equation  
 143 (2) results in additional constraints for the coupling constants such that, taking into account  
 144 energy conservation, twelve free coupling constants remain. As will be seen later, the additional  
 145 terms necessary to ensure energy conservation only play a role at the very end of the early  
 146 nonlinear phase.

147 The free coupling constants can be obtained by fitting the time evolution of the energies con-  
 148 tained in the toroidal harmonics described by Equations (1) to those resulting from a JOREK  
 149 simulation. Initial values for the coupling constants are taken from the simulations with only  
 150 two or three included toroidal harmonics. In every step of the fitting procedure, the system of  
 151 nonlinear coupled differential equations is solved and the quadratic differences of the logarithmic  
 152 energies for every harmonic and for a large set of points in time are summed and minimized.

153 Figure 4 compares the energy time traces of the JOREK simulations to the simple model with six  
 154 free parameters. It can be seen that the results of the simulation in the early nonlinear phase are  
 155 very well reproduced by the simple quadratic interaction model. The values for the six coupling  
 156 constants obtained from the fit<sup>6</sup> are close to the initial values verifying that the relevant coupling

<sup>6</sup>The coupling constants obtained from the fit are  $\gamma_{9,10}^1 = 113$ ,  $\gamma_{8,10}^2 = 76$ ,  $\gamma_{7,10}^3 = 65$ ,  $\gamma_{6,10}^4 = 21$ ,  $\gamma_{7,8}^{15} = 32$  and  
 $\gamma_{7,9}^{16} = 34$  (units omitted).

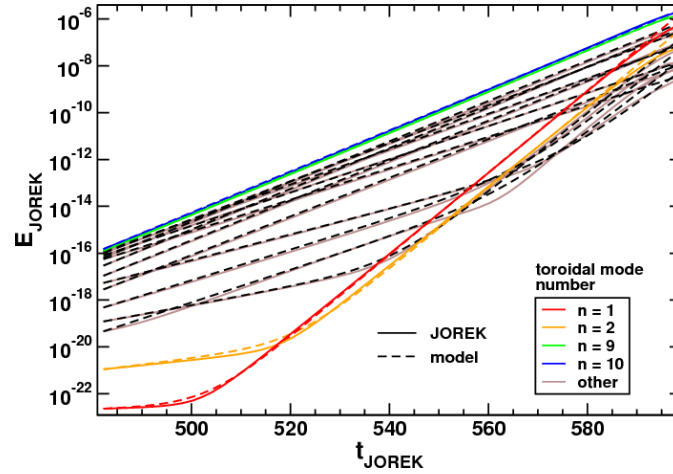


Figure 4: Time evolution of the energies contained in the toroidal Fourier harmonics of a JOREK simulation with included mode numbers  $n = 1, 2, \dots, 16$  (straight lines) compared to the results of the simple model with six free parameters (dashed lines). The model is based on the idea that energy is transferred among the toroidal harmonics due to second order nonlinear interaction between them. In the early nonlinear phase, the results from the simple model agree very well with the JOREK results. The deviations between JOREK simulation and model at the end of the early nonlinear phase correspond to the expectations as in this phase the growth is already influenced by saturation effects which are not described by the simple model.



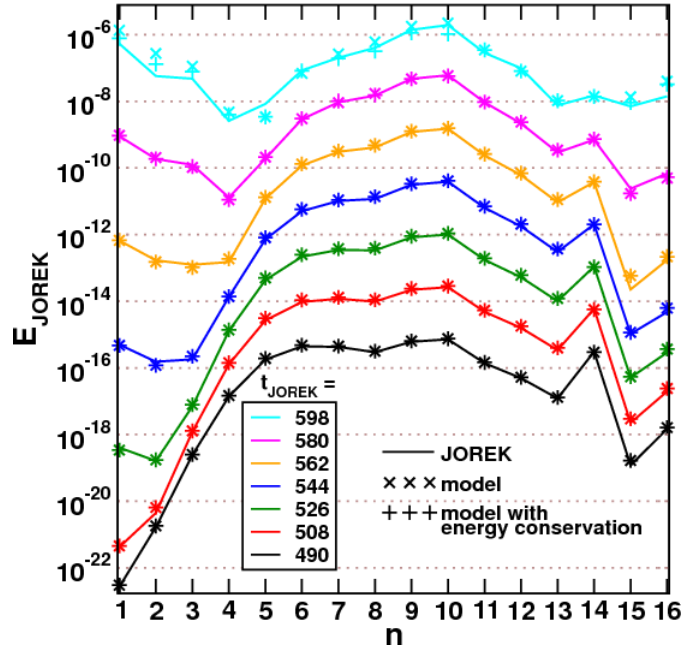


Figure 5: Energy spectrum of the toroidal Fourier harmonics in a JOREK simulation with  $n = 1, 2, \dots, 16$  (straight lines) compared to the results of the simple quadratic coupling model (crosses) for different points in time. It can be seen how the low- $n$  part of the spectrum increases significantly and the energies become comparable to those of the linearly dominant harmonics. The plot shows the results of two different versions of the model, one has six free coupling constants ( $x$ ) and the other one has twelve free coupling constants in order to account for energy conservation ( $+$ ). The results of the simple model do not deviate from the more accurate one except at the end of the early nonlinear phase.

157 constants were taken into account. From the excellent agreement using only few free parameters,  
158 it can be concluded that the early nonlinear evolution of the toroidal Fourier spectrum is indeed  
159 determined by quadratic coupling. Furthermore, it can be seen that the nonlinear growth of a  
160 driven harmonic is mainly dominated by one single nonlinear coupling term only<sup>7</sup>. As a linearly  
161 growing harmonic evolves as  $A_j(t) = A_{j,0} \exp(\gamma_j t)$ , it follows thus from Equation (1) for the  
162 growth rate of the nonlinearly driven harmonic that  $\gamma_{i,\text{nonlinear}} = d \log A_i / dt = \gamma_j + \gamma_k$ , i.e., the  
163 nonlinear growth rate of the driven harmonic equals the sum of the growth rates of the two  
164 driving harmonics.

165 The time evolution of the energy spectrum from JOREK (solid lines) and from the simple inter-  
166 action model (x) are shown in Figure 5. It is visible that at the end of the early nonlinear phase  
167 where the saturation sets in, the results from the simple model start to deviate from the JOREK  
168 results. This corresponds to the expectations, as the mechanisms responsible for the saturation  
169 are not described by the model. As the linear growth rates are assumed to be constant in the  
170 model, a reduction of the drive of the instability due to the effects described above cannot be  
171 reflected. Moreover, the assumption of rigidly growing harmonics leading to constant coupling  
172 constants, breaks down when saturation sets in. Figure 5 also shows the results from the sim-  
173 ple interaction model accounting for energy conservation (+). It can be seen that the additional  
174 terms only play a role at the end of the early nonlinear phase.

175 The simple interaction model has also been tested on two JOREK simulations with only four  
176 included toroidal harmonics ( $n = 4, 8, 12, 16$ ) and different distances between plasma and ideal  
177 wall which effectively changes the linear growth rates, but preserves the spatial structure of the  
178 toroidal harmonics. The results of both JOREK simulations are reproduced well with the simple  
179 model by only adapting the linear growth rates but keeping the same coupling constants.

180 The very good agreement indicates that the simple model provides a good explanation of the  
181 non-linear drive of low- $n$  harmonics in the JOREK simulations and could well explain the ob-  
182 servations of strong low- $n$  harmonics in the experiment [11].

## 183 **5 Evolution of the $n=1$ spatial structure**

184 In the previous section it has been shown how energy is transferred to linearly subdominant  
185 toroidal Fourier harmonics via nonlinear coupling of the dominant harmonics. It has been shown  
186 that the  $n = 1$  toroidal component can even become one of the dominant harmonics, driven by  
187 the interaction between the linearly most unstable toroidal harmonics ( $n = 9$  and  $n = 10$  in this  
188 case). In this section, the question is addressed, how the spatial structure of the  $n = 1$  harmonic  
189 in the poloidal plane is affected by this energy transfer.

---

<sup>7</sup>This corresponds to the expectations as among competing exponentially growing terms, the one with the highest growth rate will always dominate after a short period of time.

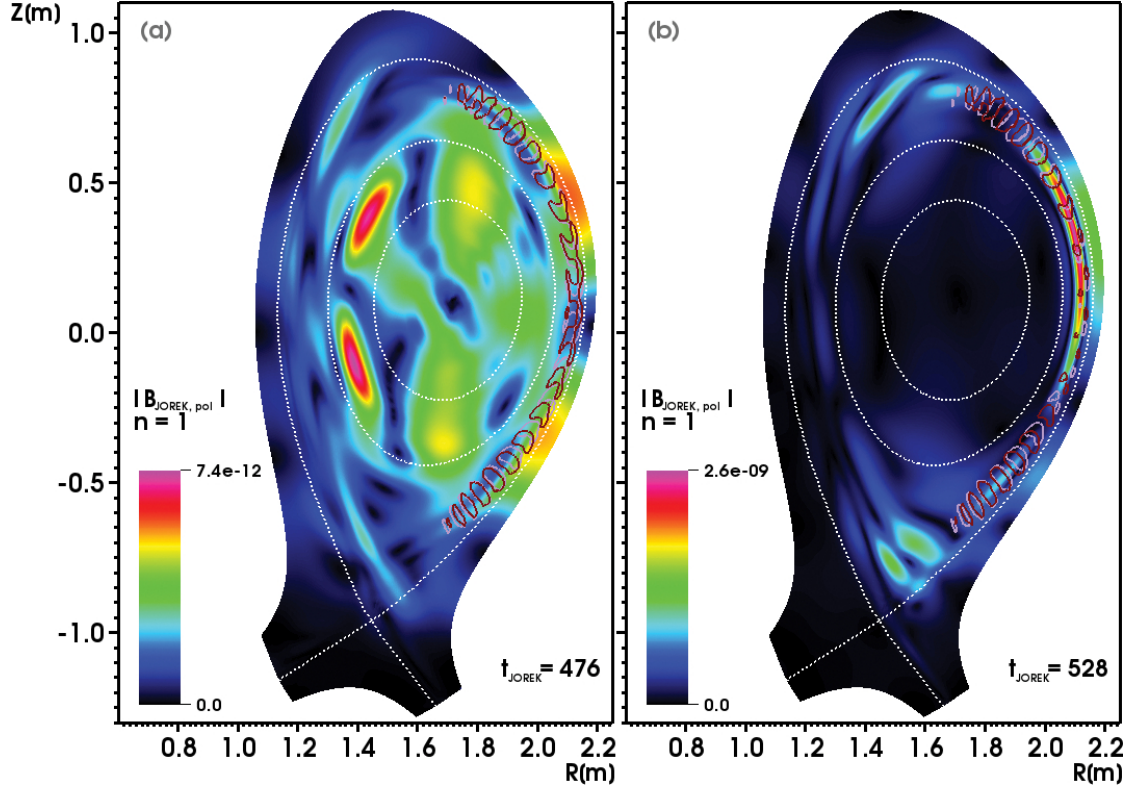


Figure 6: Poloidal cross section of the absolute value of the  $n = 1$  poloidal magnetic field perturbation in the linear phase (a) and in the early nonlinear phase (b) of a simulation with included mode numbers  $n = 1, 2, \dots, 16$ . The dotted white lines show the separatrix and flux surfaces at  $\Psi_N = 0.33$  and  $\Psi_N = 0.66$  where  $\Psi_N = (\Psi - \Psi_{\text{axis}}) / (\Psi_{\text{separatrix}} - \Psi_{\text{axis}})$  is the normalized equilibrium poloidal magnetic flux. Contours at 50% of the maximal value of the absolute value of the poloidal magnetic field perturbation are plotted in mauve for the  $n = 9$  component and in dark red for the  $n = 10$  component for comparison. In the linear phase, the  $n = 1$  toroidal harmonic extends far into the plasma core. In contrast, in the early nonlinear phase, it is radially localized at the plasma edge where also the  $n = 9$  and  $n = 10$  are maximal. The poloidal position of the  $n = 1$  on the low-field side in this phase corresponds to the poloidal region where the  $n = 9$  and  $n = 10$  are in phase.

190 Figure 6 (a) shows the absolute value of the  $n = 1$  component of the poloidal magnetic field  
191 perturbation in the linear phase of a JOREK simulation with  $n = 1, 2, \dots, 16$ . In the linear phase,  
192 the  $n = 1$  component extends over a large part of the whole plasma volume. In simulations  
193 where the  $n = 1$  harmonic is the only included toroidal harmonic, the perturbation grows rigidly  
194 preserving this structure<sup>8</sup>.

195 In contrast to the simulations with only one included toroidal harmonic, in the simulations with  
196  $n = 1, 2, \dots, 16$  the structure of the  $n = 1$  does not continue to grow rigidly. When the growth rate  
197 of the  $n = 1$  starts to increase due to nonlinear coupling, its structure changes significantly. After  
198 a phase of transition a new rigidly growing structure is observed. The rigid growth sets in when  
199 the growth rate of the  $n = 1$  is fully determined by the energy transfer from dominant harmonics.  
200 This new  $n = 1$  structure in the early nonlinear phase is shown in Figure 6 (b). It is now peaked  
201 at the edge of the plasma, in the radial region where also the  $n = 9$  and  $n = 10$  are localized. The  
202 poloidal localization of the  $n = 1$  on the low-field side coincides approximately with the region  
203 where the  $n = 9$  and  $n = 10$  are in phase<sup>9</sup>. The rigidity of the new  $n = 1$  structure is illustrated in  
204 Figure 7, where contours of the absolute value of the  $n = 1$  poloidal magnetic field perturbation  
205 are drawn for two different points in time during the early nonlinear phase.

206 The observed evolution of the  $n = 1$  spatial structure can be interpreted as a superposition of  
207 two rigidly growing structures. The first one, visible in the linear phase of the simulation, is  
208 the linearly unstable  $n = 1$  growing at a very small growth rate. The second structure, which  
209 emerges in the early nonlinear phase, corresponds to a different, linearly stable but nonlinearly  
210 driven  $n = 1$  which quickly covers the linear structure due to the much stronger growth rate.  
211 The phase of transition can indeed be approximately reproduced by superposing the two rigid  
212 structures starting at different initial amplitudes and growing at different growth rates.

## 213 6 Conclusions and Outlook

214 Nonlinear reduced MHD simulations of the early ELM phase based on ASDEX Upgrade param-  
215 eters have been presented. In order to analyze the evolution of the toroidal Fourier harmonics,  
216 emphasis has been put on simulations including a large set of toroidal harmonics and simula-  
217 tions including different combinations of these harmonics. It has been observed that linearly  
218 weakly unstable toroidal harmonics can achieve large growth rates due to nonlinear coupling of  
219 dominant harmonics. In particular the energy of the  $n = 1$  harmonic becomes comparable to en-  
220 ergies of linearly dominant harmonics in the course of the nonlinear phase, which corresponds  
221 to recent experimental observations in TCV [11]. To explain what determines this nonlinear

---

<sup>8</sup>Note, that at very low energies at the beginning of the growth, the structure of the  $n = 1$  is still oscillating both in the simulation with  $n = 1, 2, \dots, 16$  and in the simulation with only  $n = 1$ . But the further time evolution of the  $n = 1$  only simulation shows, that the structure plotted in Figure 6 (a) later becomes a rigidly growing structure.

<sup>9</sup>The poloidal angle where this is the case of course depends on the chosen toroidal position.

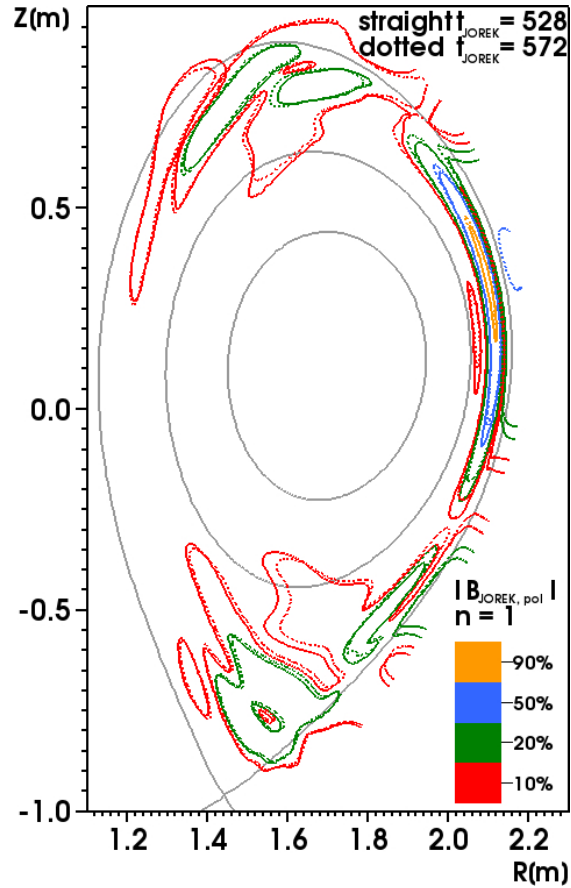


Figure 7: Contours at different fractions of the maximal absolute value of the  $n = 1$  component of the poloidal magnetic field perturbation. The structures at the beginning of the early nonlinear phase (straight lines) and shortly before nonlinear saturation sets in (dotted lines) agree very well, which shows that the structure of the  $n = 1$  toroidal harmonic shown in Figure 6 (b) grows rigidly until the onset of saturation. The grey lines show the separatrix and flux surfaces at  $\Psi_N = 0.33$  and  $\Psi_N = 0.66$ .

222 behavior of the toroidal Fourier spectrum, a simple quadratic interaction model has been set up,  
223 based on the idea that second order nonlinear coupling between toroidal harmonics can gener-  
224 ate harmonics with "sum and difference mode numbers". This model is able to reproduce to a  
225 large extent the time evolution of the toroidal energy spectrum in the early nonlinear phase of  
226 JOREK simulations before saturation sets in. In particular, the model reproduces the growth  
227 rates of the linearly driven toroidal harmonics in the early nonlinear phase. This shows, that the  
228 nonlinear evolution of the toroidal Fourier spectrum in this phase is predominantly determined  
229 by quadratic coupling. The growth of the  $n = 1$  harmonic is driven by interaction between the  
230 two linearly most unstable toroidal harmonics.

231 Furthermore, it has been investigated how the spatial structure of the  $n = 1$  in the poloidal plane  
232 is modified by the energy transfer to the  $n = 1$  in the nonlinear phase. It has been observed that  
233 the rigidly growing structure of the linearly unstable  $n = 1$  which reaches far into the plasma  
234 core transitions into another rigidly growing structure of a linearly stable but nonlinearly driven  
235  $n = 1$ . This second structure is localized at the edge of the plasma, in the region where also  
236 the two linearly dominant harmonics are maximal, which is in line with the idea that the  $n = 1$   
237 emerging in the nonlinear phase is generated by the interaction between these harmonics. The  
238 assumption brought up in Reference [11], that a strong  $n = 1$  component gives access to the  
239 plasma core, which could explain the large losses of energy observed during type-I ELMs, is  
240 thus not supported by the simulations, as nonlinearly, the  $n = 1$  becomes highly localized at the  
241 edge. Nevertheless, strong low- $n$  components could couple easier to core instabilities having a  
242 similar toroidal structure, such as neoclassical tearing modes.

243 As a next step, it would be interesting to render simulations with more realistic values for vis-  
244 cosity and resistivity possible. As diamagnetic stabilization and sheared toroidal plasma rotation  
245 are expected to have some influence on the nonlinear coupling between the toroidal harmonics,  
246 including these effects in the simulations is also planned. Moreover, simulations exceeding the  
247 early ELM phase are subject of ongoing work.

## 248 **7 Acknowledgments**

249 A part of this work was carried out using the HELIOS supercomputer system at Computational  
250 Simulation Centre of International Fusion Energy Research Centre (IFERC-CSC), Aomori,  
251 Japan, under the Broader Approach collaboration between Euratom and Japan, implemented  
252 by Fusion for Energy and JAEA. This work was partially funded by the Max-Planck/Princeton  
253 Center for Plasma Physics. K.L. would like to acknowledge the support by the Austrian Science  
254 Fund (FWF) under Grant No. P19901. The authors would also like to thank Ronald Wenninger  
255 for the discussions about the experimental findings.

## 256 References

- 257 [1] H Zohm. Edge localized modes (ELMs). *Plasma Physics and Controlled Fusion*, 38(2):  
258 105, 1996. URL <http://stacks.iop.org/0741-3335/38/i=2/a=001>.
- 259 [2] A Loarte, G Saibene, R Sartori, D Campbell, M Becoulet, L Horton, T Eich, A Herrmann,  
260 G Matthews, N Asakura, A Chankin, A Leonard, G Porter, G Federici, G Janeschitz,  
261 M Shimada, and M Sugihara. Characteristics of type I ELM energy and particle losses  
262 in existing devices and their extrapolation to ITER. *Plasma Physics and Controlled Fu-*  
263 *sion*, 45(9):1549, 2003. URL [http://stacks.iop.org/0741-3335/45/i=9/](http://stacks.iop.org/0741-3335/45/i=9/a=302)  
264 [a=302](http://stacks.iop.org/0741-3335/45/i=9/a=302).
- 265 [3] N Klimov, V Podkovyrov, A Zhitlukhin, D Kovalenko, J Linke, G Pintsuk, I Landman,  
266 S Pestchanyi, B Bazylev, G Janeschitz, A Loarte, M Merola, T Hirai, G Federici, B Ric-  
267 cardi, I Mazul, R Giniyatulin, L Khimchenko, and V Koidan. Experimental study of PFCs  
268 erosion and eroded material deposition under ITER-like transient loads at the plasma gun  
269 facility QSPA-T. *Journal of Nuclear Materials*, 415(1, Supplement):59–64, 2011. ISSN  
270 0022-3115. doi:10.1016/j.jnucmat.2011.01.013. Proceedings of the 19th International  
271 Conference on Plasma-Surface Interactions in Controlled Fusion.
- 272 [4] G T A Huysmans and O Czarny. MHD stability in X-point geometry: simulation of ELMs.  
273 *Nuclear Fusion*, 47(7):659, 2007. URL [http://stacks.iop.org/0029-5515/](http://stacks.iop.org/0029-5515/47/i=7/a=016)  
274 [47/i=7/a=016](http://stacks.iop.org/0029-5515/47/i=7/a=016).
- 275 [5] A Herrmann. Special issue: ASDEX Upgrade. *Fusion Science and Technology*, 44(3):  
276 569–742, 2003.
- 277 [6] G T A Huysmans. Non-linear MHD simulations of ELMs. In *35th EPS Con-*  
278 *ference on Plasma Phys., Hersonissos*, 2008. URL [http://epsppd.epfl.ch/](http://epsppd.epfl.ch/Hersonissos/pdf/P2_065.pdf)  
279 [Hersonissos/pdf/P2\\_065.pdf](http://epsppd.epfl.ch/Hersonissos/pdf/P2_065.pdf).
- 280 [7] O Czarny and G T A Huysmans. Bézier surfaces and finite elements for MHD simula-  
281 tions. *Journal of Computational Physics*, 227(16):7423–7445, 2008. ISSN 0021-9991.  
282 doi:10.1016/j.jcp.2008.04.001.
- 283 [8] M Hölzl, S Günter, R P Wenninger, W-C Müller, G T A Huysmans, K Lackner, I Krebs,  
284 and the ASDEX Upgrade Team. Reduced-magnetohydrodynamic simulations of toroidally  
285 and poloidally localized edge localized modes. *Physics of Plasmas*, 19(8):082505, 2012.  
286 doi:10.1063/1.4742994.
- 287 [9] P J McCarthy, P Martin, and W Schneider. The CLISTE interpretive equilibrium code. IPP-  
288 Report 5/85, Max-Planck-Institut für Plasmaphysik, Boltzmannstraße 2, 85748 Garching,  
289 Germany, 1999.
- 290 [10] P J McCarthy. Analytical solutions to the Grad–Shafranov equation for tokamak equi-  
291 librium with dissimilar source functions. *Physics of Plasmas*, 6(9):3554–3560, 1999.  
292 doi:10.1063/1.873630. URL <http://link.aip.org/link/?PHP/6/3554/1>.

293 [11] R P Wenninger, H Reimerdes, O Sauter, and H Zohm. Non-linear magnetic perturbations  
294 during edge localized modes in TCV dominated by low n mode components. submitted to  
295 Nuclear Fusion, 2013.